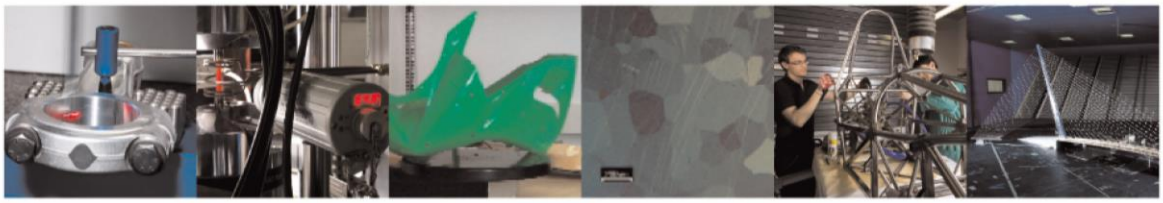

High-speed imaging and process characterization of coaxial laser metal wire deposition

Motta, Maurizio; Demir, Ali Gökhan; Previtali, Barbara

This is a post-peer-review, pre-copyedit version of an article published in ADDITIVE MANUFACTURING. The final authenticated version is available online at: http://dx.doi.org/10.1016/j.addma.2018.05.043

DIPARTIMENTO DI MECCANICA ■ POLITECNICO DI MILANO
via G. La Masa, 1 ■ 20156 Milano ■ EMAIL (PEC): pecmecc@cert.polimi.it
http://www.mecc.polimi.it
Rev. 0

High-speed imaging and process characterization of coaxial laser metal wire deposition

Maurizio Motta[1], Ali Gökhan Demir[1*], Barbara Previtali[1]

[1]Department of Mechanical Engineering, Politecnico di Milano, Via La Masa 1, 20156 Milan, Italy

*Corresponding authors; aligokhan.demir@polimi.it

High-speed imaging and process characterization of coaxial laser metal wire deposition

Maurizio Motta[1], Ali Gökhan Demir[1*], Barbara Previtali[1]

[1]Department of Mechanical Engineering, Politecnico di Milano, Via La Masa 1, 20156 Milan, Italy

Highlights

- Coaxial LMWD is studied with AISI 308 wires determining the feasibility map.
- High speed imaging with external illumination is used to analyse defects.
- Formation mechanisms of stubbing and dripping are presented.
- Power decay strategy to tackle heat accumulation in multiple layers is presented.
- Benchmark data of porosity, productivity, roughness, and microhardness is provided.

Abstract

In this work, coaxial laser metal wire deposition (LMWD) process is studied, with particular attention to defect formation mechanisms and the establishment of stable processing conditions. The coaxial LMWD of AISI 308 stainless steel wire was processed by a multi-mode fiber laser delivered to an industrial coaxial LMWD deposition head. The continuous mechanical connection with the deposition region requires further attention to the process dynamics, which may alter the deposition precision and continuity. Accordingly, this work presents a systematic analysis of how the defects are formed at single and multiple layer deposition conditions. High-speed imaging is employed to reveal the process dynamics as a diagnostics aid. The process stability is determined initially at single layer condition, providing a correct match between the melting

position and rate of the wire. At multiple layer deposition, the thermal load is managed to achieve high-aspect ratio components. At the stable conditions, the process is benchmarked for porosity, surface roughness, and deposition rates.

Keywords: Directed energy deposition; Coaxial wire feeding; Process diagnosis; Defect formation; Beam shaping

1. Introduction

Among different additive manufacturing (AM) techniques, directed energy deposition (DED) techniques provide several advantages in producing metal components . These advantages are related to the possibility of producing large size components, adding features to existing components, the use of the same process for repair, and high efficiency in material use. A primary distinction between the different processes can be related to the used energy source (*i.e*. laser, electron beam, plasma or arc) and the used feedstock (*i.e*. powder and wire) [1]. Different combination of these have been explored as means for additively producing metallic parts, where the union of the laser beam with powder feedstock has been by the far the most widely exploited one [2]. Indeed, the use of the laser beam provides flexible operation in ambient atmosphere and high precision, consisting of a compromise between the competing energy sources. The choice for the powder feedstock derives partially from the long existing research and industrial applications related to laser cladding. More importantly the use of powder allows for a straightforward approach to transport the feedstock in a continuous manner to the processing zone by means of powder feeding systems and dedicated process nozzles. Moreover, the small powder size (typically between 40 and 100 μm) can allow for adequate precision and surface quality. The introduction of fiber lasers with high brightness and flexible beam transport accelerated the pick-up of this technology in the industrial field, where the current research is exploring further possibilities related to the higher precision and new material metallurgy.

Wire as a feedstock in DED processes has been used mainly with plasma or arc energy sources. This is due to the simple transfer of common welding techniques such as metal inert gas (MIG), tungsten inert gas (TIG), and plasma towards the use for AM [3–8]. A common advantage for techniques such as MIG and plasma welding is that the wire can be fed coaxially, hence the tool tip that is defined as the union of the heat source and the feedstock is axisymmetric. Hence, the build-up of complex shapes becomes intrinsically possible. The use of an electron beam wire feedstock is also currently available in the industry (Sciaky, Inc., Chicago, Illinois, USA) [9]. The system does not accommodate the wire feed coaxially. However, by employing several number of wires laterally, axial symmetry can be improved. The use of wire feedstock with laser beams has also been a common practice in laser welding or cladding with filler wire [10–12]. Such systems commonly employ lateral wire feed, suffering from limited movement capability and reduced flexibility in the deposition geometry. Despite such disadvantage, their use in producing different material such as Ni-alloys [13–15], Ti-alloys [5,16,17], and steels [18,19] has been studied widely in the literature proving their potential for highly demanding applications such as aerospace, automotive, and biomedical

implant manufacturing. However, laser beams can be flexibly shaped to allow the insertion of a coaxial wire, which has been a more recent industrial development.

The interest for the use of wire feedstock in AM derives from many factors. The wire feedstock is achieved from a widely-established wire drawing process, where many alloys are already produced in different diameters. This is an important factor that can reduce the production costs compared to the use of powder feedstock [20]. The material usage is high (close to 100%), retaining an environmentally and economically advantageous production route for small series[21]. Moreover, the wire feedstock is intrinsically safe compared to the micro dimensional powders, which can be highly explosive and flammable. Improved precision through the use of small sized wires and pulsed wave emission has been shown to reduce the deposit dimensions to micrometric scales [22,23]. On the other hand, the use of wire feedstock with laser beam provides distinct defect types due to a constant mechanical link between the workpiece and the deposition head through the wire. In low energy conditions "stubbing" is observed, whereas excessive energy results in the so called "dripping" phenomenon [24]. The use of coaxial feeding requires further attention from this point of view as the wire feeding and beam handling is carried out by the same piece of hardware and imperfections in alignment can result in process failure [25]. To authors' knowledge, such studies have not been carried up to date.

Accordingly, this work studies the laser metal wire deposition (LMWD) process employing an industrial coaxial wire deposition head coupled to a multimode fiber laser and a robotic arm. The work investigates the deposition of 1 mm AISI 308, exploring the conditions required to achieve high aspect ratio thin-walled structures in a step-by-step manner. The experimental work is assisted by the use of high-speed imaging to reveal the defect formation in-situ at single- and multi-layer deposition cases. Finally, the process is characterized in stable conditions to provide benchmark in terms of quality and productivity.

2. Materials and methods

2.1. Material

AISI 308 stainless steel wires with 1 mm diameter were used as the feedstock material. The wires were cold drawn and annealed. The material is commonly used for welding and repair operations on stainless steel structures. As substrate material 6 mm-thick AISI 316 stainless steel plates were used. The chemical composition is shown in Table 1.

2.2. LMWD system

The LMWD system is composed of industrial equipment fit to purpose. The core of the system is a coaxial wire deposition head (Coaxcladder, Precitec, Gaggenau, Germany). The employed light source was a 3-kW multi-mode active fiber laser (YLS-3000, IPG Photonics, Cambridge, MA, USA). Feedstock was provided to the process head via an industrial wire feeding system (Abicor Binzel, Buseck, Germany). A six-axis

anthropomorphic robot (ABB IRB 2400-10, Zürich, Switzerland) with a rotary table was used as the positioning system.

The beam shaping capability of the deposition head allowed for the coaxial insertion of the wire feedstock. Before reaching the deposition head, the laser beam was launched from the feeder fiber with 50 μm diameter to a larger process fiber with 400 μm diameter fiber by means of a fiber to fiber coupler. The process fiber is connected to a collimator at the processing head inlet. At this point, the laser beam is deflected to an axicon lens, where the Gaussian distribution is changed to a ring (see Figure 1.a). The shaped beam then passes through a prism splitting it into two half-rings, providing the opening required for the wire to pass. The wire feeding is inserted through a deflecting mirror, where the processing laser is reflected towards the processing zone. After this point, the wire runs in the middle of two half-rings of the laser beam. Later, the beam shaping process is reversed, where first the two separate half-rings are connected by means of another prism. Finally, the ring-shaped laser beam passes through a focusing aspheric lens. The ring shape is projected towards the advancing wire. Due to this functioning principle, the focal point of the laser beam with respect to the position of the wire plays a crucial role in the process stability. The processing head also is equipped with an air knife to keep the optics clean and a shielding gas nozzle (see Figure 1.b). The main characteristics of the system are summarized in Table 2.

2.3. High-speed imaging system

A high-speed imaging system with synchronous external light was employed to analyse the process dynamics. The high-speed camera could provide up to 900.000 fps (Fastcam Mini AX200, Photron, San Diego, CA, USA). The sensor size is 1024 x 1024 pixels, where pixel dimension is 20 μm x 20 μm. In order to suppress the process emission and provide sufficient light during the fast acquisition of the process a pulsed diode laser emitting at 640 nm was employed (CAVILUX HF, Cavitar, Tampere, Finland). The laser provided a peak of 280 W power, with 2% maximum duty cycle.

In this work, high-speed images were acquired at 1500 fps employing the whole sensor size. The laser was placed at a lateral configuration, while the high-speed camera was used to image the reflected illuminator light. The illuminator laser is coupled to a delivery fiber terminated with a beam sizing lens, which was adjusted to illuminate the region of interest of approximately 30 mm in diameter. A band-pass filter at 640±10 nm was inserted in front of the high-speed camera. Figure 2 depicts the system configuration.

The field of view of the camera has been set to the correct height of observation according to the experimented condition. The depth of field of the used optical setup was sufficient to provide the imaged area on focus. In this work, the measurement of the melt pool size has not been the main concern, whereas it was aimed to provide an in-depth analysis to identify the defect formation mechanisms. External illumination is also useful from this point of view, where the actual molten zone can be viewed by suppressing the process emission and observing the actual geometry of the melt pool by means of the reflected light. Therefore, the melt pool position and shape was from the images in terms of the brighter zones [27].

2.3. Characterization and benchmarking

The multi-layered deposits obtained under stable conditions were further characterized. In particular, metallographic analyses were carried on cross-section prepared by conventional cutting and polishing techniques. Optical microscopy was used to analyse the material microstructure and porosity (EchoLab, Echo Research and Development, Milan, Italy). Image analysis software was used to assess the apparent density (ρ_A) [28]. Images were binarized leaving porosity zones as black and solid zones as white. The following expression was used to calculate the apparent density

$$\rho_A = \frac{A_S - A_p}{A_S} \quad (1)$$

where A_S is the cross-section area and A_p is the area of the pores. Build rate was also characterized for the same condition defined as the ratio of the total deposited volume (V_{tot}) to the total deposition time (t_{tot}). Considering that the system carries out a constant deposition track length (C) with fixed transverse speed (v_t) over the total number of layers (N), build rate (BR) can be estimated using the following equation:

$$BR = \frac{V_{tot}}{t_{tot}} = \frac{A_S C}{\frac{C}{v_t} N} = \frac{A_S v_t}{N} \quad (2)$$

Over the cross-sections, Vickers microhardness was also evaluated using 500 gf applied load and 15 s dwell time (VMHT 30A, Leica, Wetzlar, Germany). Surface roughness was measured with a tactile profilometer. Height profile along the build axis was taken over 17.5 mm length. Primary (P), roughness (R), and waviness (W) profiles were then extracted. A Gaussian filter with the cut-off frequency at 2.5 mm was used to separate the roughness and waviness components.

2.4. Experimental procedure

The experimental work was carried out step-by-step involving the phases to reach stable deposition conditions required to realize functional components. Hence, separate experimental plans involving the conditions for correct layer adherence, stable single-layer and multiple-layer depositions were analysed.
In all experiments, the main process parameters involved are related to the laser source, positioning system, and the wire feeder. In particular, laser power (P) and transverse speed (v_t) control the amount of energy released on the deposit region. Wire feed rate (v_w) controls the amount of material released over the deposition region. Focal position (f) controls the size of the beam projected on the processing zone, as well as where the laser beam hits the wire. In multi-layer deposition, the layer thickness (Δz) is also defined as the height increment applied by the positioning system at each consecutive layer. A circular trajectory with 50 mm diameter was chosen as the standard geometry for all tests.

3. Analysis of process defects and stabilization of the process

3.1. Layer adherence

As opposed to conventional laser optics, the beam shaping strategy used in the coaxial LMWD head constitutes differences in the propagation of the converging beam. After the focusing optic, the beam propagates in the form of a cone shell towards the focal point, where the wire passes in the middle. Accordingly, the union point between the laser beam and the wire plays a crucial role in the correct functioning of the process. This is firstly a geometrical issue that requires to be solved prior to any parameter study. Therefore, it was studied with a fixed set of parameters varying the focal position only.

Through preliminary analysis, it was found out that the beam focal point has to remain below the base plate surface. At this stage, laser powder was fixed at 1 kW and a transverse speed of 1 m/min was used. The wire feed rate was fixed at 1.2 mm/min. Focal position was varied between -7 and -5 mm. Process parameters are shown in Table 3.

Figure 3 shows the distinct deposition conditions obtained as a function of the focal position. It can be seen that a slight variation in the focal position results in defected conditions, where the -6 mm value appears to ensure correct adherence at the first layer. At -7 mm, the laser beam is too large on the base plate surface. Hence, the wire hits the base plate surface without receiving sufficient amount of energy. The track consists of fragments of unmelted wire, a characteristic appearance of the "stubbing condition" (Figure 3.a). At -5 mm, the laser beam reaches the wire surface above the base plate, starting the melting process at an excessive height. Accordingly, the molten material forms droplets in the absence of a complete contact with the base plate. Eventually, the droplets fall on the base plate forming the so called "dripping" condition (Figure 3.c). The track is also discontinuous due to the absence of any deposition until the first droplet falls. Instead, the focal position at -5 mm was found to be adequate for ensuring a correct adherence on the surface. The track is free of deposition defects and shows homogenous width overall (Figure 3.b). Accordingly, for further investigations, the focal position was fixed at -6 mm.

3.2. Single-track feasibility window identification

Once correct position of the focal point is established, the main process parameters that control the linear energy density on the material were varied. Liner energy density was calculated as:

$$E = \frac{P}{v_t} \tag{4}$$

During the experiments laser power was varied between 0.8 and 1.1 kW, whereas the transverse speed was varied between 0.8 and 1.1 m/min. The wire feed rate was adjusted proportionally to the transverse speed by using a constant speed ratio (r_v), which is expressed by

$$r_v = v_w / v_t \tag{3}$$

Throughout the experiments the speed ratio was 1.2. Table 4 reports the fixed and varied parameters in this phase of the study. The results were categorically analysed in terms of visual appearance of the deposited tracks. Dripping and stubbing were the main defect categories, whereas a third one namely "deposition with defects" was also defined. This condition corresponded to a transition zone between dripping and the acceptable condition referred to as "good deposition".

Figure 4 illustrates the full process map. It can be seen that the process stability is ensured at only a limited

portion of the experimented region. In particular, a minimum of 1 kW laser power is required for reaching the stability zone. As opposed to other laser based AM processes, the linear energy density appears to be ineffective in terms of representing the process variations. As shown in Figure 4, the same levels of linear energy density can produce both defected and correct deposition conditions. As an example, moving over the 60 J/mm iso- linear energy density line, the conditions change from good deposition, to deposition with defects to finally stubbing as both the power and transverse speed are decreased. Despite the fact that the wire feed rate is proportionally decreased each time, this appears to not compensate the energy required to ensure a full melting of the wire. On the other hand, with fixed power levels, a reduction of transverse speed results in deposition with defects and finally dripping, which is in agreement with LMWD works carried out with lateral feeding [24]. The formation of stubbing appears to mainly depend on the power deficiency.
In order to examine the defect formation mechanisms, it is required to analyse the stable deposition conditions first. Figure 5 exhibits a high-speed camera frame showing such conditions. During the process, the wire starts to melt at the vicinity of the surface forming a constant track, which instantly solidifies. Throughout the deposition process, the molten pool remains approximately twice the wire diameter (2 mm) without further extension or reduction.
Figure 6 shows time lapse images of the dripping defect in formation acquired with the high-speed camera. It can be seen that the melting process starts above the base plate surface, where a metal droplet is formed. A second melt pool is generated below the droplet as the remaining part of the laser beam reaches the base plate surface. The droplet size increases its size as the wire is kept feeding constantly. The droplet size exceeds 3.3 mm in diameter at maximum, before collapsing to the base plate. This process takes more than 1.5 s. The collapsed droplet remains liquid for a prolonged duration even after the laser beam proceeds over it. This process is observed in a cyclic manner in space. It can be expected that the droplet fall occurs when the gravity wins over the adhesion forces between the liquid metal and the wire. Considering the density of stainless steel at melting temperature (6.9 g/cm^3) [29] and the measured size of the droplet, detachment occurs above approximately 10 mN of gravitational force.

Figure 7 shows the time lapse images of the stubbing formation. It can be viewed that due to the low energy release, the wire is not sufficiently melted and the molten pool size on the base plate is restricted. The amount of incoming wire volume exceeds the rate of the material that is molten. Hence, the wire is bent moving it outside of the melting region. At a certain point, the wire is mechanically detached from the melt pool, resulting in a fragment of residue on the deposited zone. This process takes approximately 0.3 s, considerably faster than the dripping phenomenon. Accordingly, many fragments of incompletely molten wire residue are found on the single layer as opposed to only a few droplets found in dripping.

3.3. Multi-layer deposition

The single-layer deposition study showed a restricted feasibility region for the LMWD process. Accordingly, the multi-layer deposition was studied with a fixed parameter combination in order to understand the effect of the thermal accumulation through the layers on the process stability. Indeed, the temperature of the

deposition zone is expected to rise during the process. In powder based laser DED processes, the main defect type is observed to be due to a mismatch between the height increment and the growth rate. Hence, irregular deposits are obtained. In the particular case of coaxial LMWD, starting from stable deposition conditions, heat accumulation can mainly shift the process to dripping conditions. Indeed several parameters can be commanded to maintain the process stability in DED processes concerning the laser and feedstock related parameters[4]. The coaxial LMWD process presents several limitations related to the mechanical connection between the feedstock and the deposition region, the position of the focal point with respect to the wire position, and the wire feed rate. Such conditions render the changes related to wire feed rate, transverse speed, and focal position less feasible. The change of power levels is a relatively easier option not intervening with the amount of material being input to the working zone and the position of the beam with respect to the wire. Laser power is a key parameter for changing dimensional characteristics of the deposits as well as stabilizing DED processes employing powder and wire has been demonstrated previously [30–33]. In particular, Qiu et al used similar power management schemes to maintain part geometry in laser metal deposition[34]. Hence, laser power has been regulated in order to obtain stable processing conditions in multi-layer deposition.

The heat accumulation on the workpiece could be visible observed in terms of the change in colour due to the thermal radiation at high temperatures. The workpiece would emit in the visible band during the deposition, depicting a significant increase of temperature according to Planck's law [35]. The power decay strategy was based on preliminary trials. Staring from the initial power level of 1000 W, a gradual decrease until 900 W was found to be required to keep the workpiece free of significant thermal accumulation. The final strategy was formulated and found to be effective empirically. Accordingly, two different deposition strategies were tested in order to identify the process stability over the consecutive layers. In the "constant power" strategy, the laser power was fixed at 1 kW with 1 m/min transverse speed and these parameters were kept constant over the complete deposition process. In the "power decay" strategy, the power was reduced by 25 W steps at each 5 layers, in order to reduce the thermal load on the workpiece. Layer thickness was set as 0.55 mm, which was the measured value for a single layer deposit of the same condition. A total of 24 layers were produced. Process parameters in multi-layer deposition experiments are shown in Table 5.

Figure 8 shows the differences between the two strategies regarding different layers. It can be viewed that the process remains stable for both cases until the 16^{th} layer, where the dripping defect is present at 24^{th} layer with the constant power strategy.

High-speed camera images were used as an aid to understand the defect formation mechanism. Figure 9 (a) and Figure 9 (b) show frames of the deposition of the 8^{th}, 16^{th} and layer respectively with constant power strategy. It can be seen that the molten pool enlarges both at the front and rear sides with respect to the deposition direction compared to the first layer (see Figure 5). As the layers proceed the melt front also advances along the wire. At the 24^{th} layer, the molten pool enlarges to a critical extent, where the wire detaches from the workpiece (see Figure 10). A droplet of molten metal is formed, which is later on detached

similar to the case observed with the single layer defect. Once the defect manifests, it becomes repetitive and a a new droplet forms on the tip of the wire before reaching the surface (as shown in Figure 11).

Indeed, the use of the power decay strategy avoids this defect by maintaining the thermal load. As seen in Figure 12, the molten pool is relatively longer than the one observed at the first layer, while remaining constant throughout the process. The power is lowered to 975, 925 and 900 W respectively at 8^{th}, 16^{th} and 24^{th} layers avoid significant heat accumulation. The use of such strategy has been effective on a closed contour with relatively small track length. Evidently, more complex paths would require more sophisticated strategies. However, the results indicate that the use of online temperature measurements employing techniques such as pyrometry is fundamentally important for the process. On the other hand, the implementation of such device through the optical path of the head with the dedicated beam shaping optics requires further attention.

3.3. Quality and productivity assessment

Figure 13 shows the details of a thin-walled cylindrical structure obtained with the power decay strategy employing 50 layers. As seen in the cross-section view along the build direction in Figure 13.a, the deposited component is free of macroscopic defects. The apparent density was measured to be >99.9%. The deposit shows homogenous surface texture mainly due to the layered structure of the material both in the outer and inner side of the walls. Table 6 reports the average (Pa,Ra,Wa) and the maximum height (Pt, Rt, Wt) of all the profiles have been calculated. The surface quality is evaluated often using different indicators in the literature. An objective comparison is therefore hard to be made. Regarding the components built by powder based laser DED processes, the review of Gu et al. indicates an interval for average roughness between Ra=20-90 µm depending on the employed machine configuration and material [2]. A narrower average surface roughness is indicated by the review of Vayre et al. for the powder based laser DED processes with Ra=10-25 µm [36]. On the other hand, Rombouts et al report Rt=27-37 µm for the surface roughness of AISI 316L components produced by the same process [37]. On Ti6Al4V, Gharbi et al. report the surface roughness as Rt=50-70 µm and Wt=75-200 µm [31]. The results obtained in this study show that the surface quality of LMWD components is in the range of the best surface quality reported in the literature concerning powder based DED processes.

Figure 14 exhibits the microhardness profile of the deposited cylinder over the build direction. In order to assess the homogeneity, the hardness profile was taken on both sides of the cylinder. The microhardness profile shows an identical behaviour on both sides. The hardness values drop from the vicinity of the substrate a height of approximately 5 mm, reaching an asymptotic value of 150 HV. Figure 15 shows corresponding material microstructure at the bottom, middle, and top sections of the deposits. The microstructures show that around the substrate a fine microstructure is transformed into a columnar structure following the build direction around the middle section. It can be expected that the cooling rates are much higher due to the lower initial temperature of the process around the first layers. As the process progresses,

the workpiece temperature also increases allowing for a slower cooling cycle, following the direction of the deposition. Similarly, the microhardness profile is expected to show the region where the workpiece temperature reaches an equilibrium state.

The build rate employing the developed strategy for multi-layer LMWD deposition was estimated as 59 cm^3/h. For powder based laser DED processes, different values are reported in literature and also in industrial sources. Vayre et. al declare build rates between 10 and 70 cm^3/h [36], while the reference values for stainless steel are given by the pioneering works in the field and are comparable to those achieved reported by Vayre et al [38].

4. Conclusions

This work demonstrated the use of an industrial coaxial LMWD deposition system with a fiber laser and 1 mm AISI 308 wire. The work described the various passages required to ensure stable processing conditions on multi-layered components, highlighting the defect types and their formation mechanisms in this new technology. The main conclusions of the work are as follows:

- Two main types of defects occur in the process similar to the more conventional LMWD processes namely dripping and stubbing. However, their presence was observed in distinct conditions belonging to the coaxial LMWD. In particular, the focal position is critical for a correct adherence. The wire melting should be carried out at the correct height to avoid stubbing and dripping. During multi-layer deposition, the process may drift from stable conditions, where dripping occurs in the form of detachment from the already formed molten pool.
- High-speed camera images were used as an aid for the process comprehension. The formation of both stubbing and dripping was observed in detail. The images show that the molten pool can advance both in rear and forward directions as well as towards the wire. A stable molten pool size is crucial for maintaining the contact between the wire and the workpiece. For this purpose, power decay strategies or close-loop temperature control is required.
- Under stable deposition conditions, the surface quality of the deposits is comparable to the powder DED counterparts. High density components with high productivity can be achieved. The components show a homogenous yet anisotropic microstructure.
- The work also provides insights for future online monitoring applications. The timescales and the dimensions of the observed defects can be used as cues for designing a monitoring module with adequate sampling rates. The use of external illumination always remains as an advantageous tool for revealing the melt poll geometry, whereas thermal emission of the process can also be used simplifying the setup.

Evidently, the coaxial LMWD provides an increased flexibility over the obtainable geometries. Compared to the powder DED process, the distinct defect types require a different type of reasoning for part programming and process monitoring. Sensorization of the wire feeding mechanism is also one of the possibilities that requires further attention. The thermal load was found to be an important factor on also the material

microstructure. Further empirical and modelling studies are required to assess deposition strategies to have a greater control over the material properties.

Acknowledgements

The authors acknowledge Precitec for technical support provided during the experiments. BLM Group, Andrea Crosato, Daniele Colombo, and Mauro Penasa are gratefully acknowledged for high-speed imaging system support. This work was supported by Autonomous Province of Trento through the Regional Law 6/98. Name of the granted Project: LT4.0, Linea 2: Infrastrutturazione Fisica e Digitale", project TUBE under the call "Accordi per la Competitività", and the project MADE4LO under the call "POR FESR 2014-2020 ASSE I - AZIONE I.1.B.1.3"..

References

[1] D. Ding, Z. Pan, D. Cuiuri, H. Li, Wire-feed additive manufacturing of metal components: technologies, developments and future interests, Int. J. Adv. Manuf. Technol. 81 (2015) 465–481. doi:10.1007/s00170-015-7077-3.

[2] D.D. Gu, W. Meiners, K. Wissenbach, R. Poprawe, Laser additive manufacturing of metallic components: materials, processes and mechanisms, Int. Mater. Rev. 57 (2012) 133–164. doi:10.1179/1743280411Y.0000000014.

[3] S. Jhavar, N.K. Jain, C.P. Paul, Development of micro-plasma transferred arc (μ-PTA) wire deposition process for additive layer manufacturing applications, J. Mater. Process. Technol. 214 (2014) 1102–1110. doi:10.1016/j.jmatprotec.2013.12.016.

[4] A. Heralić, A.-K. Christiansson, B. Lennartson, Height control of laser metal-wire deposition based on iterative learning control and 3D scanning, Opt. Lasers Eng. 50 (2012) 1230–1241. doi:http://dx.doi.org/10.1016/j.optlaseng.2012.03.016.

[5] E. Brandl, B. Baufeld, C. Leyens, R. Gault, Additive manufactured Ti-6A1-4V using welding wire: Comparison of laser and arc beam deposition and evaluation with respect to aerospace material specifications, Phys. Procedia. 5 (2010) 595–606. doi:10.1016/j.phpro.2010.08.087.

[6] D. Ding, Z. Pan, D. Cuiuri, H. Li, A multi-bead overlapping model for robotic wire and arc additive manufacturing (WAAM), Robot. Comput. Integr. Manuf. 31 (2015) 101–110. doi:10.1016/j.rcim.2014.08.008.

[7] J. Gockel, J. Beuth, K. Taminger, Integrated control of solidification microstructure and melt pool dimensions in electron beam wire feed additive manufacturing of ti-6al-4v, Addit. Manuf. 1 (2014) 119–126. doi:10.1016/j.addma.2014.09.004.

[8] O.T. Ola, F.E. Doern, A study of cold metal transfer clads in nickel-base INCONEL 718 superalloy, Mater. Des. 57 (2014) 51–59. doi:10.1016/j.matdes.2013.12.060.

[9] Sciaky Inc, (n.d.). http://www.sciaky.com (accessed January 5, 2017).

[10] G. Yang, J. Ma, B.E. Carlson, H.P. Wang, M.M. Atabaki, R. Kovacevic, Decreasing the surface roughness of aluminum alloy welds fabricated by a dual beam laser, Mater. Des. 127 (2017) 287–296. doi:10.1016/j.matdes.2017.04.085.

[11] E. Capello, D. Colombo, B. Previtali, Repairing of sintered tools using laser cladding by wire, J. Mater. Process. Technol. 164–165 (2005) 990–1000. doi:10.1016/j.jmatprotec.2005.02.075.

[12] E. Capello, B. Previtali, The influence of operator skills, process parameters and materials on clad

shape in repair using laser cladding by wire, J. Mater. Process. Technol. 174 (2006) 223–232. doi:10.1016/j.jmatprotec.2006.01.005.

[13] B. Baufeld, Mechanical properties of INCONEL 718 parts manufactured by shaped metal deposition (SMD), J. Mater. Eng. Perform. 21 (2012) 1416–1421. doi:10.1007/s11665-011-0009-y.

[14] D. Clark, M.R. Bache, M.T. Whittaker, Shaped metal deposition of a nickel alloy for aero engine applications, J. Mater. Process. Technol. 203 (2008) 439–448. doi:10.1016/j.jmatprotec.2007.10.051.

[15] N.I.S. Hussein, J. Segal, D.G. McCartney, I.R. Pashby, Microstructure formation in Waspaloy multilayer builds following direct metal deposition with laser and wire, Mater. Sci. Eng. A. 497 (2008) 260–269. doi:10.1016/j.msea.2008.07.021.

[16] R.M. Miranda, G. Lopes, L. Quintino, J.P. Rodrigues, S. Williams, Rapid prototyping with high power fiber lasers, Mater. Des. 29 (2008) 2072–2075. doi:10.1016/j.matdes.2008.03.030.

[17] B. Baufeld, E. Brandl, O. Van Der Biest, Wire based additive layer manufacturing: Comparison of microstructure and mechanical properties of Ti-6Al-4V components fabricated by laser-beam deposition and shaped metal deposition, J. Mater. Process. Technol. 211 (2011) 1146–1158. doi:10.1016/j.jmatprotec.2011.01.018.

[18] W.U.H. Syed, A.J. Pinkerton, L. Li, Combining wire and coaxial powder feeding in laser direct metal deposition for rapid prototyping, Appl. Surf. Sci. 252 (2006) 4803–4808. doi:10.1016/j.apsusc.2005.08.118.

[19] J. Su, M. Xiao, Z. Zhang, Z. Ye, X. Jin, Y. Yang, Microstructural morphology and evolution of austenite stainless steel deposited using pulsed laser and wire, Int. J. Adv. Manuf. Technol. (2017). doi:10.1007/s00170-017-0625-2.

[20] M. Baumers, P. Dickens, C. Tuck, R. Hague, The cost of additive manufacturing: Machine productivity, economies of scale and technology-push, Technol. Forecast. Soc. Change. 102 (2016) 193–201. doi:10.1016/j.techfore.2015.02.015.

[21] A.C.M. Bekker, J.C. Verlinden, Life cycle assessment of wire + arc additive manufacturing compared to green sand casting and CNC milling in stainless steel, J. Clean. Prod. 177 (2018) 438–447. doi:10.1016/j.jclepro.2017.12.148.

[22] A.G. Demir, Micro laser metal wire deposition for additive manufacturing of thin-walled structures, Opt. Lasers Eng. 100 (2018). doi:10.1016/j.optlaseng.2017.07.003.

[23] F. Brueckner, M. Riede, F. Marquardt, R. Willner, A. Seidel, S. Thieme, F. Brueckner, M. Riede, F. Marquardt, Process characteristics in high-precision laser metal deposition using wire and powder

Process characteristics in high-precision laser metal deposition using wire and powder, 22301 (2017). doi:10.2351/1.4983237.

[24] T.E. Abioye, J. Folkes, A.T. Clare, A parametric study of Inconel 625 wire laser deposition, J. Mater. Process. Technol. 213 (2013) 2145–2151. doi:10.1016/j.jmatprotec.2013.06.007.

[25] M. Motta, M. Penasa, A.G. Demir, A. Crosato, B. Previtali, Coaxial Laser Metal Wire Deposition of stainless steel : process characterization, in: 39th MATADOR Conf., 2017: pp. 1–7.

[26] Washko S.D., G. Aggen, Wrought Stainless Steels, in: ASM Handbook, Vol. 1, ASM International, 1990: pp. 841–907.

[27] C. Freitag, T. Arnold, M. Boley, S. Faas, F. Fetzer, C. Hagenlocher, A. Heider, M. Jarwitz, R. Weber, T. Graf, Observation of Laser Materials Processing by Means of High-Speed Imaging, in: Micro-World Obs. by Ultra High-Speed Cameras, 2017: pp. 207–225.

[28] A.B. Spierings, M. Schneider, R. Eggenberger, Comparison of density measurement techniques for additive manufactured metallic parts, Rapid Prototyp. J. 17 (2011) 380–386. doi:10.1108/13552541111156504.

[29] K.C. Mills, Fe - 316 Stainless Steel, in: Recomm. Values Thermophys. Prop. Sel. Commer. Alloy., Elsevier, 2002: pp. 135–142. doi:10.1533/9781845690144.135.

[30] T.E. Abioye, D.G. McCartney, A.T. Clare, Laser cladding of Inconel 625 wire for corrosion protection, J. Mater. Process. Technol. 217 (2015) 232–240. doi:10.1016/j.jmatprotec.2014.10.024.

[31] M. Gharbi, P. Peyre, C. Gorny, M. Carin, S. Morville, P. Le Masson, D. Carron, R. Fabbro, Influence of various process conditions on surface finishes induced by the direct metal deposition laser technique on a Ti-6Al-4V alloy, J. Mater. Process. Technol. 213 (2013) 791–800. doi:10.1016/j.jmatprotec.2012.11.015.

[32] M. Kottman, S. Zhang, J. McGuffin-Cawley, P. Denney, B.K. Narayanan, Laser Hot Wire Process: A Novel Process for Near-Net Shape Fabrication for High-Throughput Applications, Jom. 67 (2015) 622–628. doi:10.1007/s11837-014-1288-1.

[33] F. Caiazzo, Additive manufacturing by means of laser-aided directed metal deposition of titanium wire, Int. J. Adv. Manuf. Technol. (2018) 1–9. doi:10.1007/s00170-018-1760-0.

[34] C. Qiu, G.A. Ravi, C. Dance, A. Ranson, S. Dilworth, M.M. Attallah, Fabrication of large Ti-6Al-4V structures by direct laser deposition, J. Alloys Compd. 629 (2015) 351–361. doi:10.1016/j.jallcom.2014.12.234.

[35] P.R.N. Childs, Practical Temperature Measurement, Elsevier, 2001.

[36] B. Vayre, F. Vignat, F. Villeneuve, Metallic additive manufacturing: State-of-the- art review and prospects, Mech. Ind. 13 (2012) 89–96.

[37] M. Rombouts, G. Maes, W. Hendrix, E. Delarbre, F. Motmans, Surface finish after laser metal deposition, Phys. Procedia. 41 (2013) 810–814. doi:10.1016/j.phpro.2013.03.152.

[38] W.U.H. Syed, A.J. Pinkerton, L. Li, A comparative study of wire feeding and powder feeding in direct diode laser deposition for rapid prototyping, Appl. Surf. Sci. 247 (2005) 268–276. doi:10.1016/j.apsusc.2005.01.138.

List of figures

Figure 1. a) The functioning principle of the coaxial deposition head with the beam shaping optics. b) The employed experimental setup.

Figure 2. a) Schematic view of the high-speed imaging setup. b) The implemented setup.

Figure 3. The effect of focal position to the layer adherence stability.

Figure 4. Process feasibility map showing the position of different defects and stable deposition conditions.

Figure 5. A high-speed camera image showing stable deposition conditions.

Figure 6. High-speed camera images showing the formation of dripping defect.

Figure 7. High-speed camera images showing the formation of stubbing defect.

Figure 8. Appearance of the deposits obtained with the different deposition strategies as a function of layer number.

Figure 9. Evolution of the molten pool at a) 8^{th} layer and b) 16^{th} layer with constant power equal.

Figure 10. Formation of dripping at 24^{th} layer with 1 kW constant power.

Figure 11. Repetitive dripping phenomenon at 24^{th} layer with 1 kW constant power.

Figure 12. Stable processing conditions with power decay at a)8^{th}, b) 16^{th}, and c) 24^{th} layer.

Figure 13. a) Cross-section, b) macroscopic view of the outer and c) inner wall of the multi-layer deposition

Figure 14. Microhardness profile of multi-layer deposition.

Figure 15. Microstructure of multi-layer deposition at a) top, b) middle section, and c) bottom of the of the deposition.

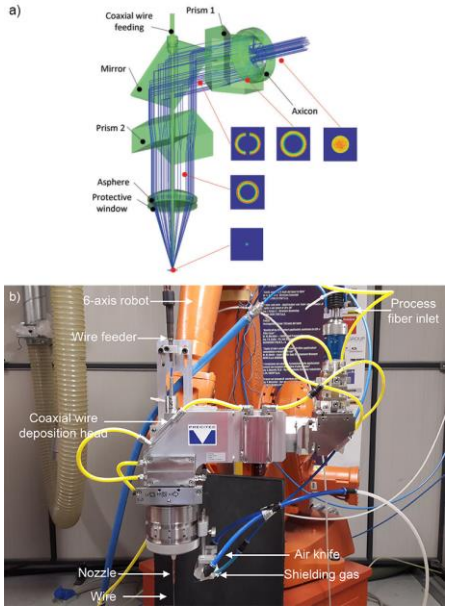

Figure 1. a) The functioning principle of the coaxial deposition head with the beam shaping optics. b) The employed experimental setup.

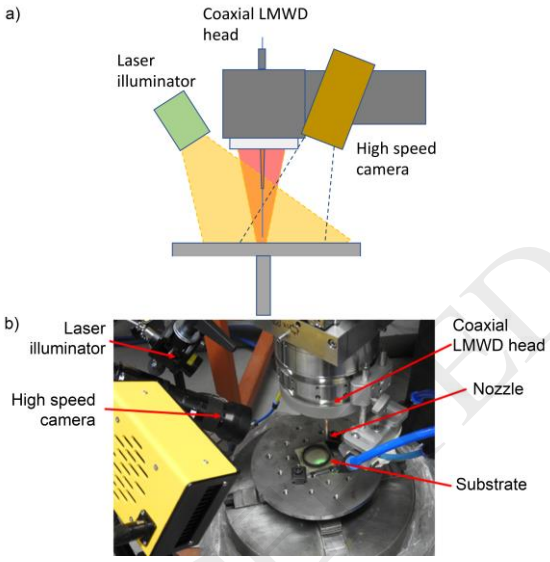

Figure 2. a) Schematic view of the high-speed imaging setup. b) The implemented setup.

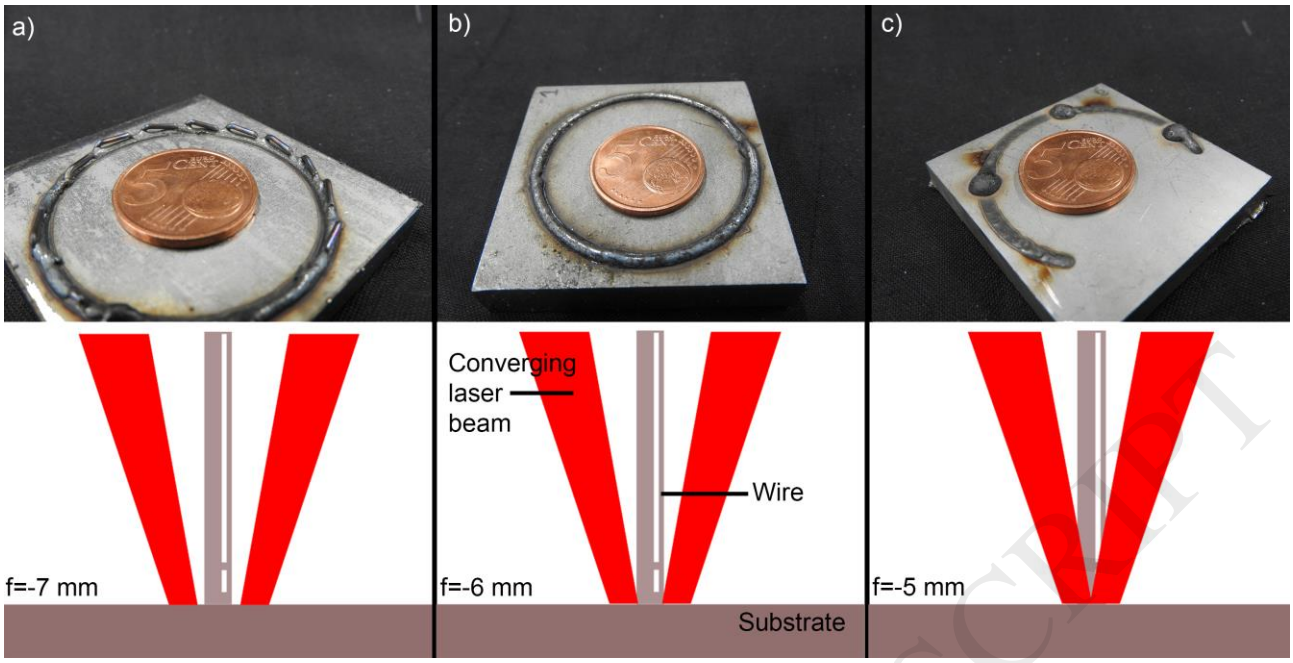

Figure 3. The effect of focal position to the layer adherence stability.

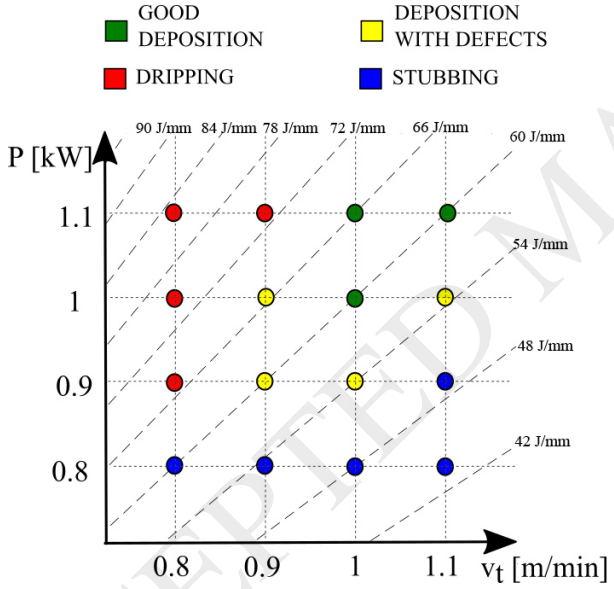

Figure 4. Process feasibility map showing the position of different defects and stable deposition conditions.

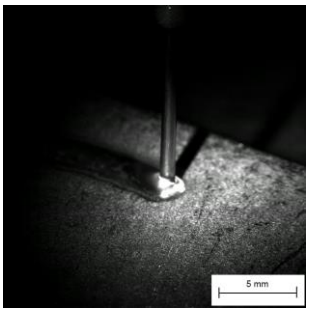

Figure 5. A high-speed camera image showing stable deposition conditions.

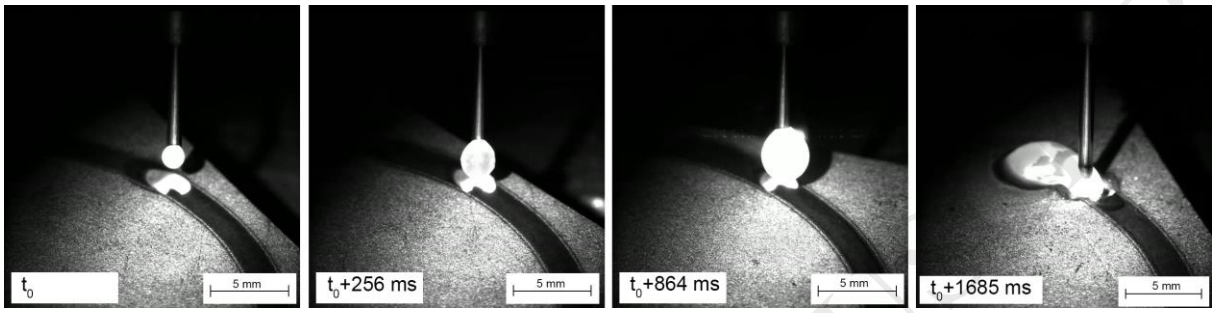

Figure 6. High-speed camera images showing the formation of dripping defect.

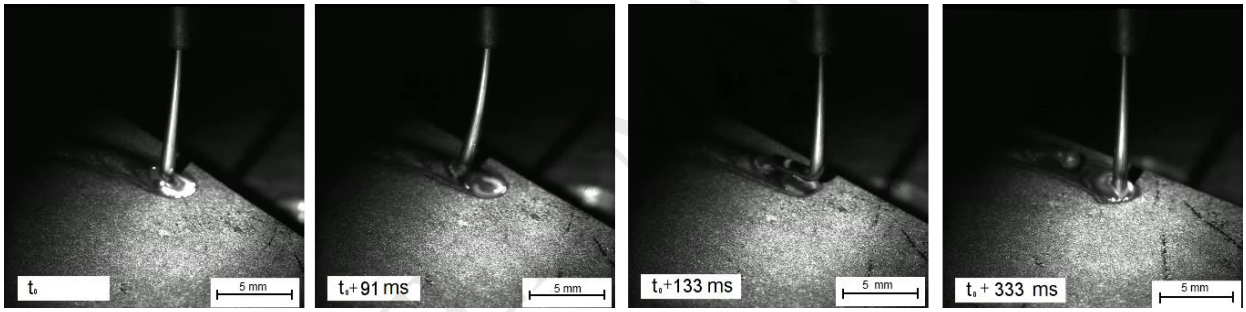

Figure 7. High-speed camera images showing the formation of stubbing defect.

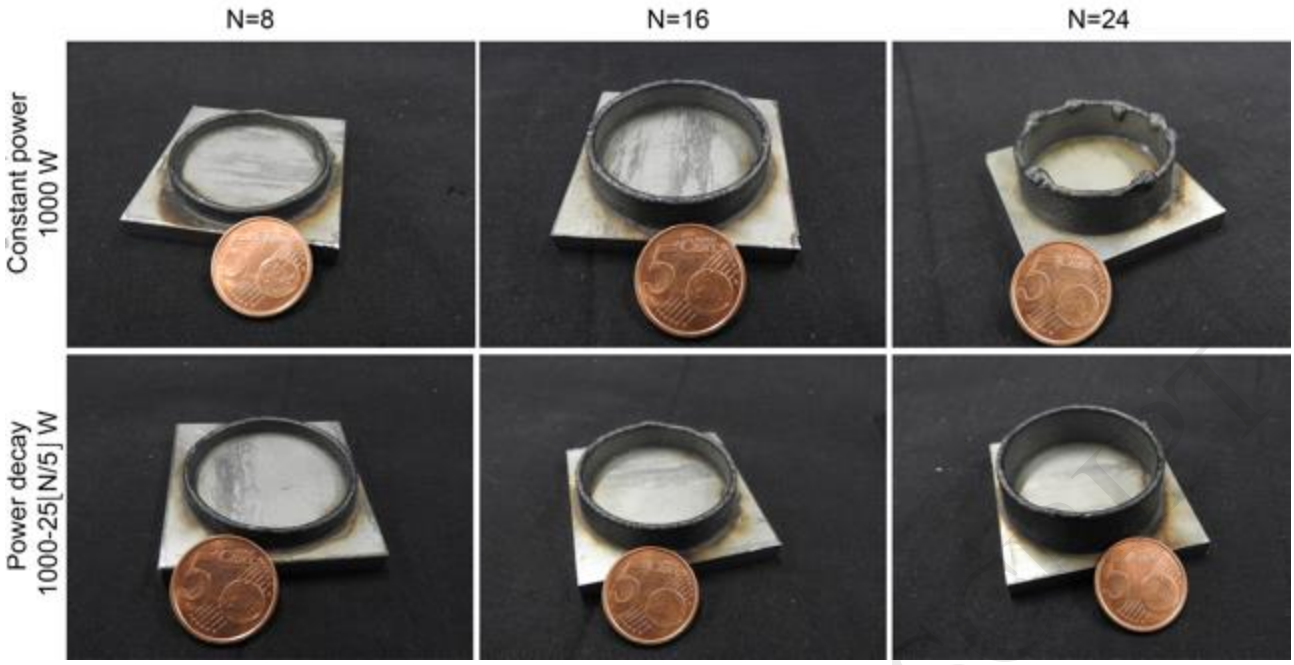

Figure 8. Appearance of the deposits obtained with the different deposition strategies as a function of layer number.

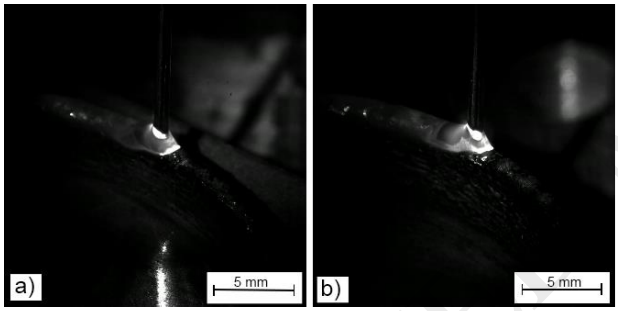

Figure 9. Evolution of the molten pool at a) 8th layer and b) 16th layer with constant power equal.

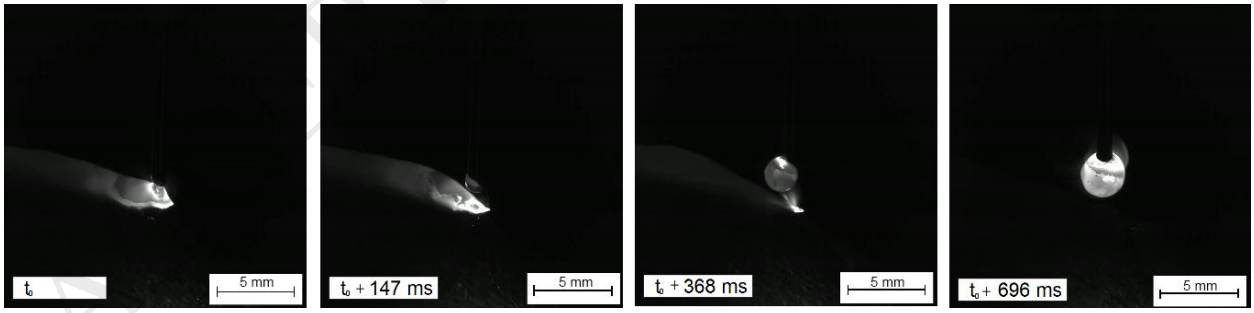

Figure 10. Formation of dripping at 24th layer with 1 kW constant power.

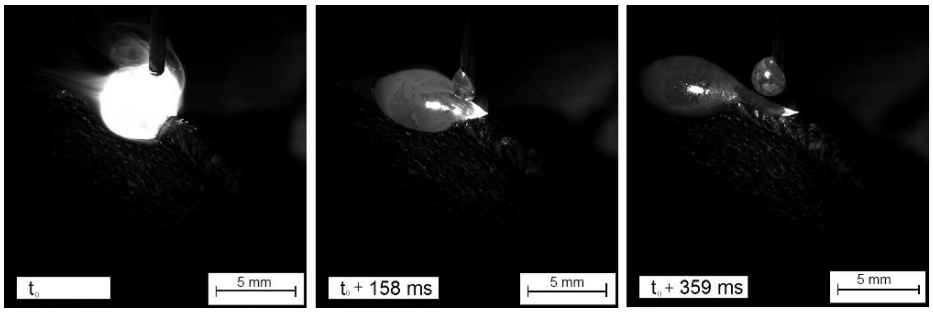

Figure 11. Repetitive dripping phenomenon at 24th layer with 1 kW constant power.

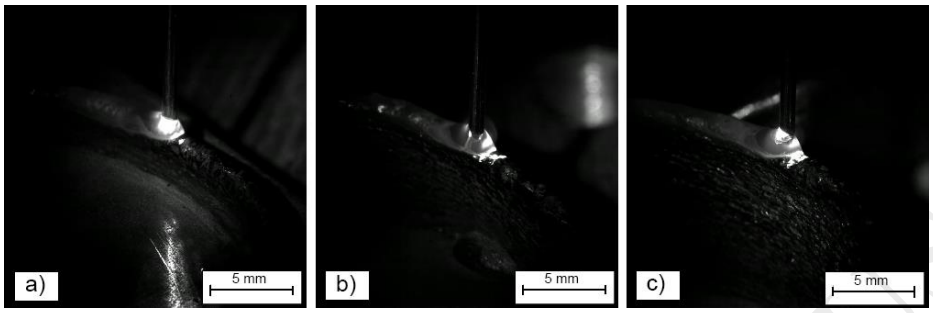

Figure 12. Stable processing conditions with power decay at a)8th, b) 16th, and c) 24th layer.

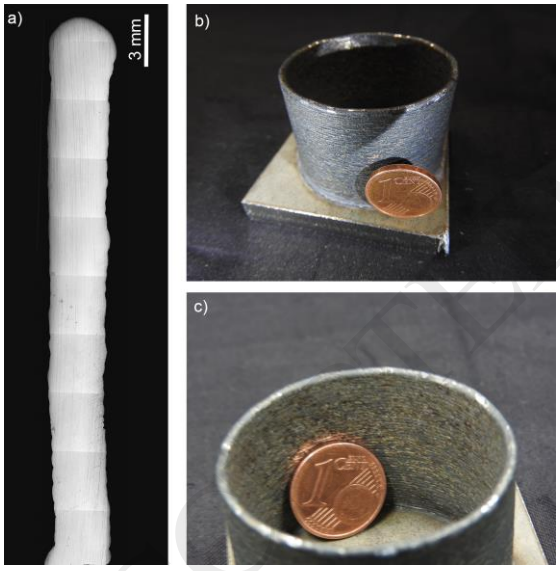

Figure 13. a) Cross-section, b) macroscopic view of the outer and c) inner wall of the multi-layer deposition.

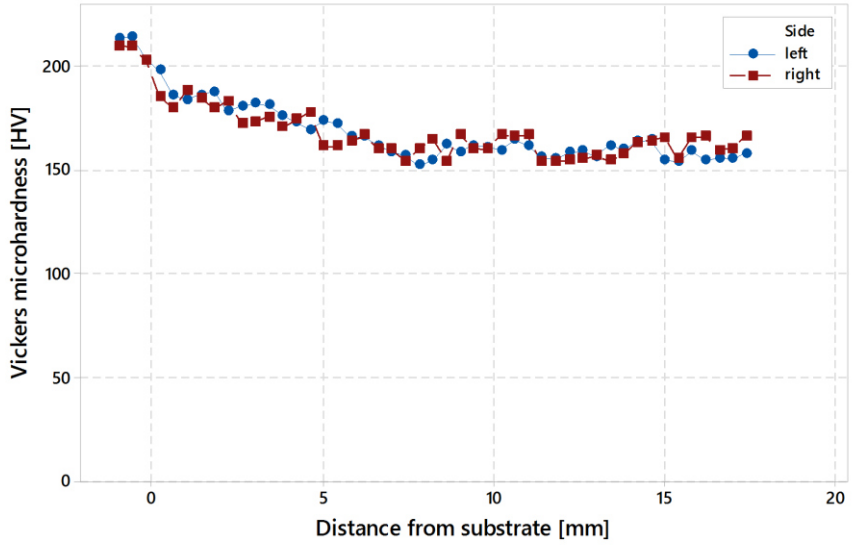

Figure 14. Microhardness profile of multi-layer deposition.

Figure 15. Microstructure of multi-layer deposition at a) top, b) middle section, and c) bottom of the of the deposition.

List of tables

Table 1. Nominal chemical composition of the wire and substrate materials [26].

Table 2. Main characteristics of the LMWD system.

Table 3. Fixed and varied parameters in the layer adherence tests.

Table 4. Fixed and varied parameters in the single-track feasibility window tests.

Table 5. Fixed and varied parameters in the study of multi-layer depositions experiments.

Table 6. Profile, roughness and waviness measurements of multi-layer deposition.

Table 1. Nominal chemical composition of the wire and substrate materials [26]**.**

wt%	C	Si	Mn	P	S	Cr	Mo	Ni	Fe
AISI 308	0.08	1	2	0.045	0.03	19-21	-	10-12	Bal.
AISI 316	0.08	0.75	2	0.045	0.03	16-18	2-3	10-14	

Table 2. Main characteristics of the LMWD system.

Parameter	**Value**
Maximum power	3 kW
Emission wavelength (λ)	1070 nm
Feeding fiber diameter	50 μm
Process fiber diameter	400 μm
Diameter at focal point (d_0)	1.7 mm
BPP (feeding fiber)	1.9 mm·mrad
Wire diameter	1 mm

Table 3. Fixed and varied parameters in the layer adherence tests.

Fixed parameters	**Value**		
Power (P)	1000 W		
Traverse speed (v_f)	1 m/min		
Wire feed rate (v_w)	1.2 m/min		
Shielding gas	Ar at 6 bar		
Varied parameters	**Levels**		
Focal position (f)	-7 mm	-6 mm	-5 mm

Table 4. Fixed and varied parameters in the single-track feasibility window tests.

Fixed parameters	**Value**			
Speed ratio (r_v)	1.2			
Focal position (f)	-6 mm			
Shielding gas	Ar at 6 bar			
Varied parameters	**Levels**			
Traverse speed (v_t) [m/min]	0.8	0.9	1	1.1
Power (P) [W]	800	900	1000	1100

Table 5. Fixed and varied parameters in the study of multi-layer depositions experiments.

Fixed parameters	**Value**	
Traverse speed (v_t)	1 m/min	
Wire feed rate	1.2 m/min	
Shielding gas	Ar at 6 bar	
Layer thickness (Δz)	0.55 mm	
Number of layers, N	24	
Varied parameters	**Levels**	
	Constant power	Power decay
Power (P) [W]	1000	1000-25* ⌊N/5⌋

Table 6. Profile, roughness and waviness measurements of multi-layer deposition.

Parameter	**Inner wall**	**Outer wall**
Pa [μm]	22.3±2.9	21.1±3.8
Pt [μm]	158.9±34.6	143.7±23.8
Ra [μm]	12.1±0.7	11.2±1.2
Rt [μm]	94.4±18.7	72.5±14.2
Wa [μm]	13.7±4.0	10.9±2.7
Wt [μm]	60.3±17.4	48.2±11.8